https://doi.org/10.15407/exp-oncology.2025.03.377

B. Partsvania [1, *], T. Sulaberidze [1], A. Khuskivadze [2], S. Abazadze [2], T. Gogoladze [1]

[1] Georgian Technical University, Institute of Cybernetics, Tbilisi, Georgia
[2] Geogia-Israel Joint Clinic "Gidmrdi"

* Correspondence: Email: besarion.partsvania@gtu.ge

UTILIZING INFRARED IMAGING TO EVALUATE THE AGGRESSIVENESS OF PROSTATE CANCER

Background. Prostate cancer (PCa) remains a leading cause of cancer-related deaths among men. While PSA screening has reduced mortality, the lack of its specificity and limitations of biopsy necessitate alternative diagnostic approaches. **Aim**. To evaluate the aggressiveness of PCa using an infrared (IR) imaging technique to improve PCa detection and treatment planning. **Materials and Methods**. We conducted a study using IR imaging on formalin-fixed paraffin-embedded prostate tissue samples from 60 patients who underwent radical prostatectomy. An IR-sensitive CCD camera, a holder for the sample, and an IR irradiation source (LED 850 nm) are parts of the experimental setup. Custom software was used to analyze tissue samples. For each aggressiveness group (low, intermediate, high; n = 20 per group), the ratio of average illumination (RAI) between malignant and healthy regions was calculated. **Results.** RAIs between malignant area and healthy areas for different aggressiveness levels (mean ± 95% CI) were low-aggressiveness [6.8—7.2], intermediate [5.2—6.1], and high-aggressiveness [4.4—5.0]. These intervals did not overlap. The control (benign) tissues showed RAI > 7.5. The method demonstrated a sensitivity of 88% and specificity of 91% in distinguishing highly aggressive tumors. **Conclusion.** IR imaging reliably differentiates PCa aggressiveness, with non-overlapping RAI intervals for each group. This technique may enhance early detection and guide personalized treatment strategies.

Keywords: prostate cancer, infrared imaging, aggressiveness, diagnosis.

Prostate cancer (PCa) is the second most common cause of cancer-related death among men worldwide, following lung cancer, and represents a significant public health challenge [1, 2]. Over the past decades, the introduction of prostate-specific antigen (PSA) screening has contributed to the reduction in PCa mortality by approximately 20% [3—5]. However, despite these advances, PCa remains a leading cause of cancer-related death, in part due to the limitations of the current diagnostic methods.

PSA testing, while sensitive, lacks specificity; elevated PSA levels can result from benign prostatic hyperplasia, prostatitis, or other non-malignant conditions [6—9]. Consequently, many men undergo unnecessary biopsies, which are invasive and may still miss early-stage cancer due to the small size or focal nature of malignant lesions.

Citation: Chekhun V, Burda T. Mushii O. Pavlova A. Borikun T, Zadvornyi T, Lukianova N. Stress-induced modulation of the tumor microenvironment: mechanisms and implications for cancer progression. *Exp Oncol.* 2025; 47(3): 377-384. https://doi.org/10.15407/exp-oncology.2025.03.377

These diagnostic gaps underscore the need for improved, non-invasive, and reliable methods to detect and characterize PCa, especially in its early stages. A critical aspect of PCa management is distinguishing between aggressive and indolent tumors [10, 11].

An accurate assessment of the tumor aggressiveness is essential for guiding treatment decisions, minimizing overtreatment, and improving patient outcomes. The current imaging modalities, such as multiparametric MRI and molecular markers, have enhanced diagnostic accuracy but remain limited by cost, accessibility, and the need for specialized expertise [12—16].

Infrared (IR) imaging has emerged as a promising, instrument-based alternative diagnostic method. Our previous studies have demonstrated the feasibility of using IR imaging to detect PCa by exploiting the differences in the optical properties of malignant and healthy tissues [17—20]. However, the earlier versions of our IR imaging device were unable to differentiate between varying degrees of tumor aggressiveness, limiting their clinical utility.

The present study aims to address this gap by evaluating the potential of IR imaging not only to detect PCa but also to assess its aggressiveness. By quantifying the ratio of the average illumination (RAI) between malignant and healthy tissue regions in formalin-fixed paraffin-embedded (FFPE) prostate samples, we seek to establish objective, non-overlapping RAI intervals corresponding to different grades of PCa aggressiveness. This approach may offer a rapid, non-destructive adjunct to conventional histopathology, facilitating more precise risk stratification and individualized treatment planning for patients with PCa.

Materials and Methods

Patient samples and ethical approval. This study was conducted on prostate tissue samples obtained from 60 patients (mean age 67 ± 8 years; range 52—78 years) who underwent radical prostatectomy at the Georgia-Israel Joint Clinic "Gidmedi" between 2022 and 2024. All participants provided written informed consent before inclusion in the study. The protocol was approved by the Independent Local Ethical Commission of the Georgia-Israel Joint Clinic "Gidmedi" (ILEC ID NO: 35). For control purposes, 10 benign prostate tissue samples from patients undergoing surgery for non-malignant conditions were also included.

Fig. 1. Schematic of the experimental setup showing a CCD camera over and IR LEDs under the prostate tissue sample

Tissue preparation and histopathology. After surgery, prostate samples were fixed in 10% neutral buffered formalin and embedded in paraffin. Sections of 5—6 μm thickness were cut and mounted on glass slides for the histopathological analysis. All slides were reviewed independently by two board-certified pathologists, blinded to the imaging results, and graded using the Gleason scoring system according to the current guidelines. The most prevalent and secondary patterns were recorded for each case.

IR imaging system. The experimental setup consisted of an IR-sensitive CCD camera, an IR source, and a custom-designed tissue holder. The IR source was positioned under the sample, while the camera was mounted over it. The camera output was digitized and transferred to a computer for analysis (Fig. 1).

The equipment specification was as follows:

- Camera: IR 1000, DAGE-MTI Co.; pixel size 6.45 μm; spectral sensitivity 400—1000 nm. Image acquisition: 16-bit grayscale, 2048 × 2048 pixels

Fig. 2. FFPE prostate sample and the corresponding stained histology section, illustrating shape concordance

• IR source: LED array, 850 nm, LED 850 nm, irradiating angle 130, radiant intensity 1 mW/sr at 20 mA, invisible to humans

• Software: Custom Python 3.9 application with OpenCV and NumPy libraries.

Image analysis and software algorithms. The custom software automatically segmented malignant and healthy regions in each IR image using adaptive thresholding and region-growing algorithms. Regions of interest (ROIs) were defined based on coordinates mapped from the corresponding histopathology slides. The software calculated the mean pixel intensity for malignant and healthy ROIs. All measurements were performed in triplicate for each sample to assess reproducibility.

Experimental design and blinding. For each Pca aggressiveness (low, intermediate, high) group (n = 20 per group), at least 20 independent experiments were performed. Control (benign) samples were analyzed similarly. All image analyses were conducted by operators blinded to the histopathological classification.

Statistical analysis. Statistical analysis was performed using SPSS version 27 (IBM Corp., USA). RAI values were summarized as means with 95% confidence intervals (CI). Group comparisons were made using Student's *t*-test. *P*-values < 0.05 were considered statistically significant. The reproducibility of RAI measurements was assessed using the intra-class correlation coefficient (ICC).

Experiments. The distribution pattern of cancer structures and their aggressiveness is consistent in both FFPE and SMG samples. Fig. 2 illustrates one of the FFPE samples alongside its corresponding SMG. PCa cells are graded on a scale based on their microscopic appearance, following the guidelines established in [21].

The Gleason score is calculated using two primary grades assigned to the cancerous tissue: the primary grade represents the most common pattern of cancer cells identified in the sample, and the secondary grade indicates the next most prevalent pattern observed. The Gleason score combines these two grades to provide a comprehensive assessment of the cancer's aggressiveness.

IR investigations were conducted on the FFPE samples. The sequence of the experimental steps was as follows: first, the SMG was examined under a microscope to identify the predominant pattern of cancer cells. This particular SMG was used only once, specifically to analyze its prevalent pattern, which allowed us to determine the grade of cancer aggressiveness. We identified the areas (coordinates) with this prevalent pattern of malignancy on the SMG. Understanding the complementary nature of SMG and FFPE samples, we were able to determine the coordinates for both the malignant and healthy tissue on the FFPE with ease. We investigated FFPE using our setup, shown in Fig. 1. We were able to identify darker regions that correspond to malignant tissue, since we knew from our previous work that in IR images, malignant tissue appears darker than noncancerous tissue.

Our software also highlighted the areas corresponding to healthy tissues in IR images. It measured the average brightness for both areas separately and calculated RAI using. An example of our software's discrimination of the area in the IR image that corresponds to malignant tissue is shown in Fig. 3.

In total, we conducted at least 20 experiments for each grade of aggressiveness separately. Then, the software calculated the RAI ranges for each aggressiveness separately with a 95% probability (95% CI).

Results

Fig. 4 presents the IR images derived from one of the FFPE samples. The histopathological analysis of this prostate tissue reveals the presence of low-aggressive adenocarcinoma, classified under ICD code 8140/3, which accounts for 15% of the prostate volume. PCa is apparent by dark spots. The healthy tissue is represented by light patches surrounding the observed dark portions.

We examined the SMG associated with this FFPE sample under a microscope. We observed the sites that corresponded to the dark spots in the IR image. Besides, we observed the areas related to the healthy tissue. The corresponding morphological images are given in Fig. 5.

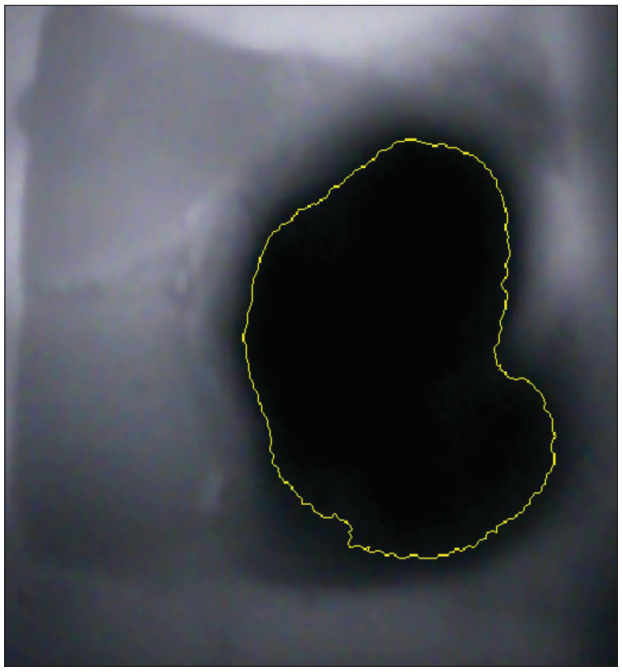

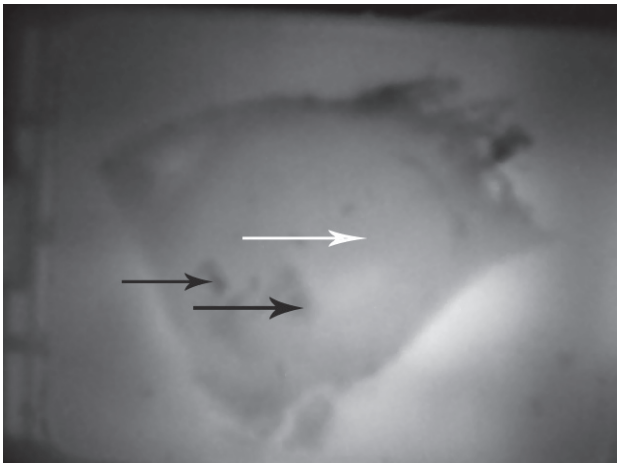

Fig. 3. IR image of prostate tissue; the cancerous region is outlined with a software-generated yellow line

Fig. 4. IR image of a lowly aggressive PCa sample. Dark areas (black arrows) indicate a tumor; the bright area (white arrow) indicates healthy tissue

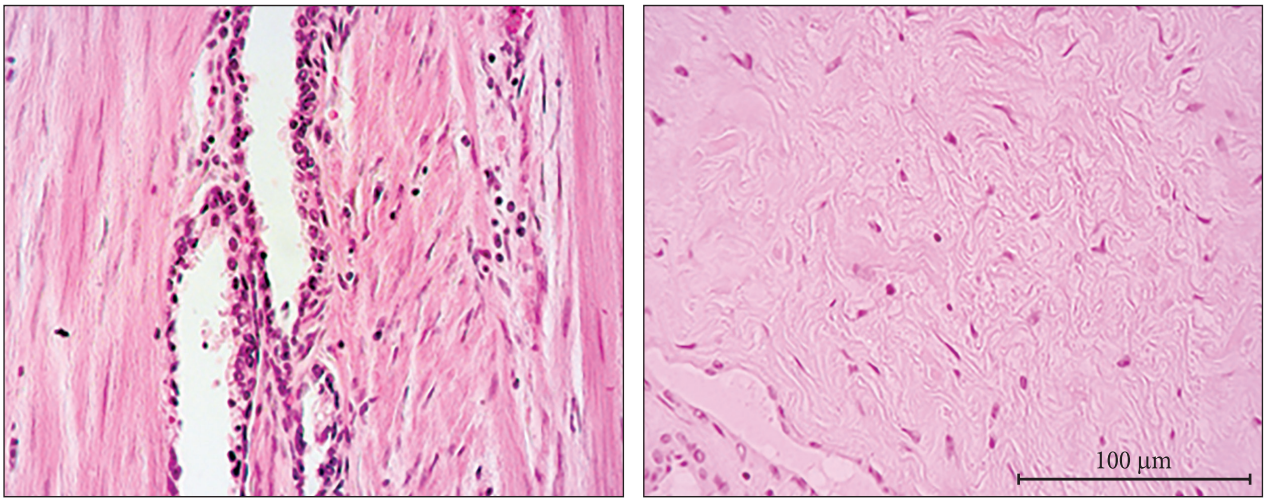

Fig. 5. Left: Histology of the tumor area from Fig. 4 (black arrow). Right: Histology of the healthy area (white arrow). ×400. Caliber 100 μm

The IR image of another FFPE sample is shown in Fig. 6. This sample exhibited cancer with intermediate aggressiveness. The dark area with the black arrow in the center corresponds to cancerous tissue, while the area indicated by the light arrow corresponds to healthy tissue. In this case, atypical polymorphic cells with vesicular nuclei were found in 30% of the prostate volume, and these cells were closely packed together. Fig. 7 presents examples of histomorphological images of both malignant and healthy tissues taken from the SMG corresponding to this FFPE. The microscopic examination of the SMG associated with this FFPE was performed standardly.

As the aggressiveness of the cancer increases, the corresponding area on the IR image becomes darker.

Fig. 8 shows the IR image of the FFPE sample with high PCa aggressiveness.

Histomorphological images of a highly aggressive PCa tissue sample, alongside the histomorphological image of a healthy tissue, are demonstrated in Fig. 9.

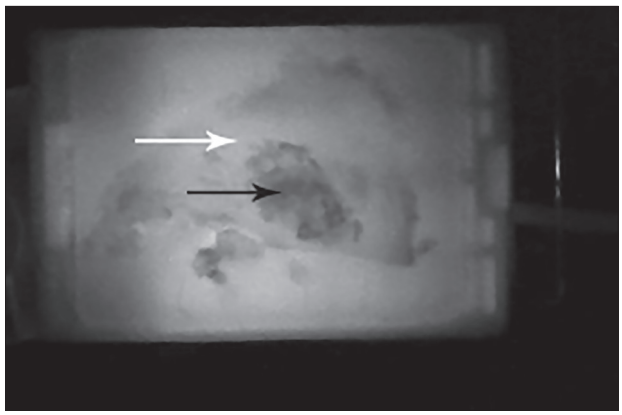

Fig. 6. IR image of a sample with intermediate aggressiveness. Dark area (black arrow) is a tumor; bright area (white arrow) is healthy tissue.

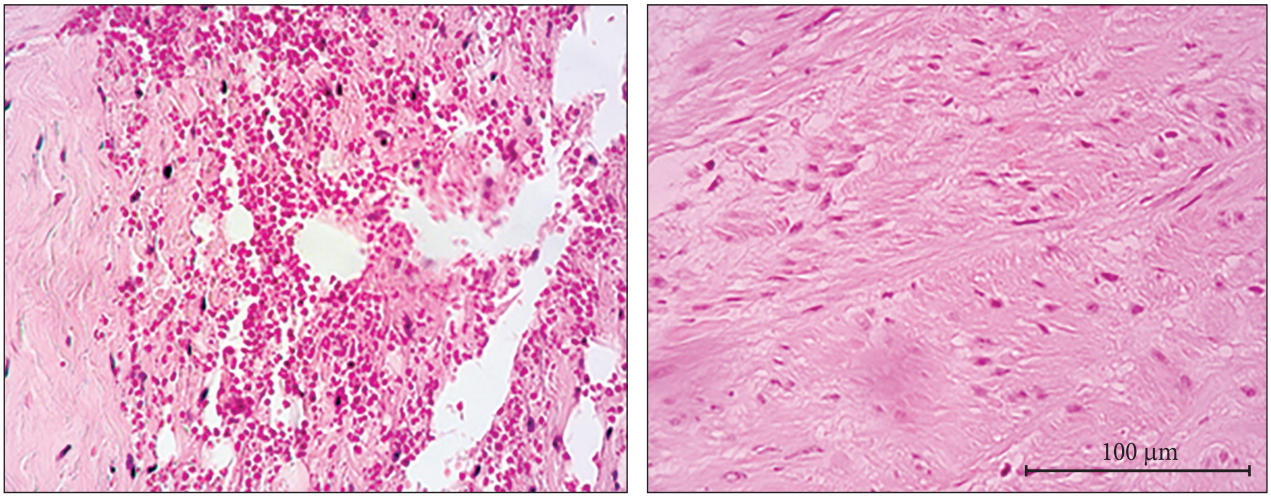

Fig. 7. Left: Histology of the intermediately aggressive tumor (black arrow, Fig. 6). Right: Healthy tissue (white arrow). ×400. Caliber 100 μm

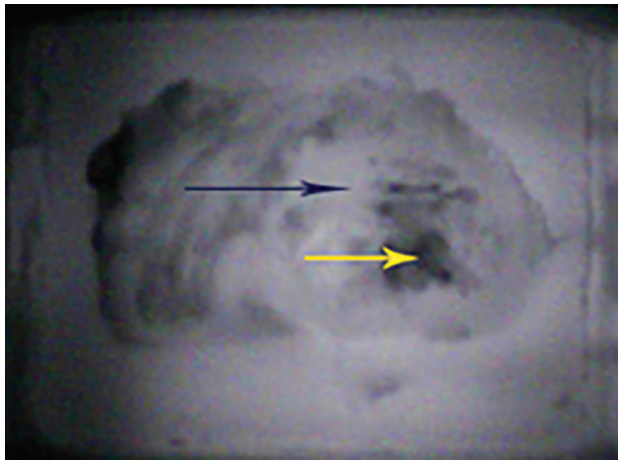

Fig. 8. IR image of highly aggressive PCa. The central dark area (light arrow) is a tumor; the peripheral area (black arrow) is healthy tissue.

After every 20 experiments, the software calculated the RAI intervals separately for each of the three aggressiveness grades.

A total of 60 cancerous and 10 benign FFPE prostate tissue samples were analyzed. For each aggressiveness group, 20 independent experiments were performed. The mean RAI values and 95% CI for each group are presented in Table 1.

The IR images revealed that malignant regions appeared darker than the healthy tissue. As the aggressiveness increased, the malignant regions became progressively darker. These findings were confirmed by the histopathological analysis, with

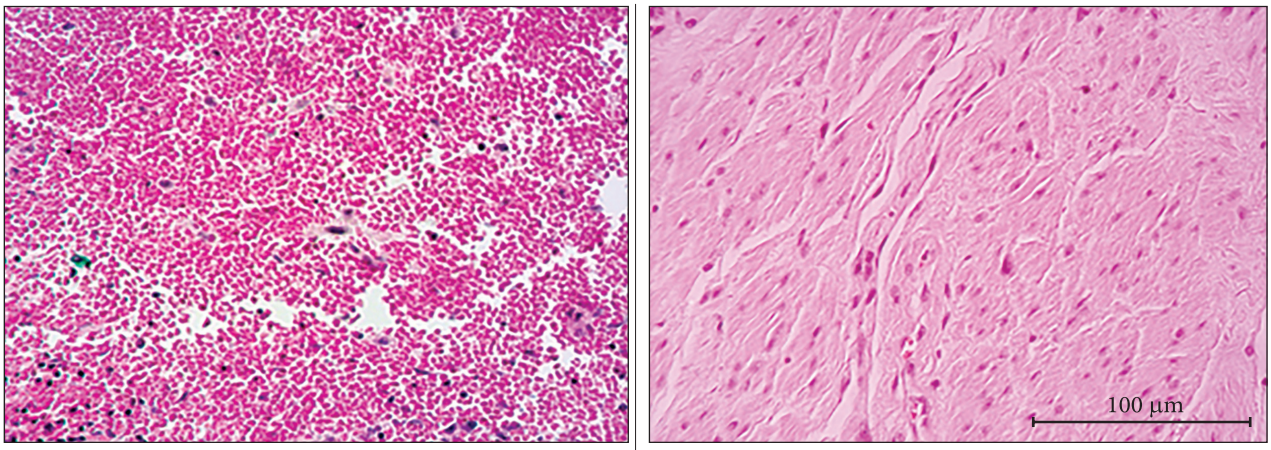

Fig. 9. Left: Histology of highly aggressive tumor area (light arrow, Fig. 8). Right: Healthy tissue (black arrow). ×400. Caliber 100 μm

mapped coordinates matching between the IR images and microscopic slides.

Triplicate measurements for each sample yielded an ICC of 0.92, indicating excellent reproducibility. All analyses were performed blinded to the histopathological grade.

Discussion

This study demonstrates that IR imaging can reliably differentiate between the varying degrees of PCa aggressiveness in FFPE tissue samples. The RAI values for low, intermediate, and high aggressiveness were non-overlapping, supporting the method's potential for objective and quantitative risk stratification.

Compared to the established diagnostic modalities such as multiparametric MRI and molecular markers, IR imaging offers several advantages: it is rapid, cost-effective, and can be performed on routine FFPE samples without specialized reagents or extensive operator training. The quantitative nature of the RAI metric enables providing clear discrimination between the aggressiveness categories, which could be particularly valuable for surgical planning and personalized treatment strategies.

However, several limitations must be acknowledged. The study sample size, while sufficient for proof-of-concept, limits generalizability. Some technical factors, such as tissue fixation, section thickness, and alignment accuracy, may affect the IR measurements. Additionally, while the ICC demonstrated high reproducibility, external validation in independent laboratories is required.

In summary, our findings indicate that IR imaging is a promising adjunct to conventional histopathology for assessing PCa aggressiveness. Future studies should focus on larger, multicenter cohorts and direct comparison with MRI and molecular diagnostics to further establish clinical utility.

Acknowledgments

This work was supported by Shota Rustaveli National Science Foundation of Georgia (SRNSFG), grant number FR-22-195. Project Title "Development of the new infrared imaging method for avoiding cancer recurrence after radical prostatectomy and partial nephrectomy."

Conflict of interest

The authors declare no conflict of interest.

Table 1. **RAI values in the groups with different PCa aggressiveness**

Group	n	RAI (Mean [95% CI])	*p*-value (adjacent group)
Low PCa aggressiveness	20	[6.8—7.2]	< 0.001
Intermediate PCa aggressiveness	20	[5.2—6.1]	< 0.001
High PCa aggressiveness	20	[4.4—5.0]	< 0.001
Benign (control)	10	[7.5—8.1]	

REFGERENCES

1. Siegel RL, Miller KD, Fuchs HE, Jemal A. Cancer statistics, 2025. *CA Cancer J Clin*. 2025;75(1):7-33. https://doi.org/10.3322/caac.21871
2. Sung H, Ferlay J, Siegel RL, et al. Global cancer statistics 2020: GLOBOCAN estimates of incidence and mortality worldwide for 36 cancers in 185 countries. *CA Cancer J Clin*. 2021;71(3):209-249. https://doi.org/10.3322/caac.21660
3. American Cancer Society. Key statistics for prostate cancer. Atlanta: American Cancer Society; 2023. Available from: https://www.cancer.org/cancer/prostate-cancer/about/key-statistics.html
4. World Health Organization. Global cancer burden growing, amidst mounting need for services. Geneva: WHO; 2024 Feb 1. Available from: https://www.who.int/news/item/01-02-2024-global-cancer-burden-growing--amidst-mounting-need-for-services
5. Ferlay J, Ervik M, Lam F, et al. Global Cancer Observatory: Cancer Today. Lyon, France: International Agency for Research on Cancer; 2020. Available from: https://gco.iarc.fr/today
6. Schröder FH, Hugosson J, Roobol MJ, et al. Prostate-cancer mortality at 11 years of follow-up. *N Engl J Med*. 2012;366(11):981-990. https://doi.org/10.1056/NEJMoa1113135.
7. Hugosson J, Carlsson S, Aus G, et al. Mortality results from the Göteborg randomised population-based prostate-cancer screening trial. *Lancet Oncol*. 2010;11(8):725-732. https://doi.org/10.1016/S1470-2045(10)70143-7.
8. Martin RM, Donovan JL, Turner EL, et al. Effect of a low-intensity PSA-based screening intervention on prostate cancer mortality: the CAP randomized clinical trial. *JAMA*. 2024;331(17):1717-1727. https://doi.org/10.1001/jama.2024.3549.
9. Roobol MJ, Carlsson SV. Screening for prostate cancer. *Hematol Oncol Clin North Am*. 2020;34(2):221-236. https://doi.org/10.1016/j.hoc.2019.11.007.
10. Pinsky PF, Prorok PC, Kramer BS. Prostate cancer screening — a perspective on the current state of the evidence. *N Engl J Med*. 2017;376(15):1457-1464. https://doi.org/10.1056/NEJMra1611696.
11. Cherney K. Aggressive Prostate Cancer: What it is and How It's Treated. Healthline, 2023. Available from: https://www.healthline.com/health/prostate-cancer/aggressive-prostate-cancer
12. Cooperberg MR, Carroll PR. Trends in management for patients with localized prostate cancer, 1990–2013. *JAMA*. 2015;314(1):80-82. https://doi.org/10.1001/jama.2015.6820
13. Giganti F, Allen C, Emberton M, et al. Factors influencing variability in the performance of multiparametric magnetic resonance imaging in detecting clinically significant prostate cancer: a systematic literature review. *Eur Urol Oncol*. 2020;3(2):145-167. https://doi.org/10.1016/j.euo.2019.12.0061
14. Jansen BHE, Oudshoorn FHK, Tijans AM, et al. Local staging with multiparametric MRI in daily clinical practice: diagnostic accuracy and evaluation of a radiologic learning curve. *World J Urol*. 2018;36(8):1201-1207. https://doi.org/10.1007/s00345-018-2295-6
15. Schoots IG, Petrides N, Giganti F, et al. Magnetic resonance imaging in prostate cancer detection: A systematic review and meta-analysis of diagnostic accuracy. *Eur Urol*. 2025;87(1):45-56. https://doi.org/10.1016/j.eururo.2024.11.005
16. de Rooij M, Hamoen EHJ, Fütterer JJ, et al. Accuracy of multiparametric MRI for prostate cancer detection: a meta-analysis. *AJR Am J Roentgenol.* 2014;202(2):343-351. https://doi.org/10.2214/AJR.13.11046
17. Turkbey B, Rosenkrantz AB, Haider MA, et al. Multiparametric MRI for prostate cancer detection and risk stratification: a critical review. *Radiology*. 2019;292(2):343-356. https://doi.org/10.1148/radiol.2019182460
18. Partsvania B, Sulaberidze T, Khuskivadze A, Abazadze S. Prostate cancer diagnostics modeling using the infrared imaging method. *Exp Oncol*. 2024;46(3):268-272. https://doi.org/10.15407/exp-oncology.2024.03.268.
19. Partsvania B, Petriashvili G, Fonjavidze N. Possibility of using near infrared irradiation for early cancer diagnosis. *Electromagn Biol Med*. 2014;33(1):18-20. https://doi.org/10.3109/15368378.2013.783845.
20. Khuskivadze A, Partsvania B, Kochiashvili D. Visualization of human prostate cancer using infrared radiation. *Urology*. 2014;84(4 Suppl):S304.
21. Abazadze S, Khuskivadze A, Kochiashvili D, Partsvania B. Dependence of prostate tissue permeability on the wavelength of radiation in the infrared range of the spectrum. *Georgian Med News*. 2021;(321):111-115.
22. Epstein JI, Zelefsky MJ, Sjoberg DD, et al. A Contemporary Prostate Cancer Grading System: A validated alternative to the Gleason score. *Eur Urol*. 2016;69(3):428-435. https://doi.org/10.1016/j.eururo.2015.06.046.

Submitted: February 02, 2025

Б. Партсванія [1], Т. Сулаберідзе [1],
А. Кхусківадзе [2], С. Абазадзе [2], Т. Гоголадзе [1]

[1] Грузинський технічний університет,
Інститут кібкрнетики, Тбілісі, Грузія
[2] Грузинсько-ізраїльська спільна клініка "Гідмрді"

ЗАСТОСУВАННЯ ІНФРАЧЕРВОНОЇ ВІЗУАЛІЗАЦІЇ ДЛЯ ОЦІНЮВАННЯ АГРЕСИВНОСТІ РАКУ ПЕРЕДМІХУРОВОЇ ЗАЛОЗИ

Стан питання. Рак передміхурової залози є провідною причиною смерті від онкологічних захворювань у чоловіків. Хоча скринінг на ПСА знизив показники смертності, низька специфічність та обмеження щодо біопсії вимагають пошуку альтернативних методів діагностики. **Мета**. Застосувати візуалізацію в інфрачервоному світлі (ІЧ) для оцінювання агресивності раку передміхурової залози для покращання діагностики та планування лікування. **Матеріали та методи**. ІЧ візуалізацію проводили на зразках фіксованої та заключеної у парафін тканини передміхурової залози у зразках, отриманих при простатектомії 60 хворих (середній вік 67 ± 8 років). Застосовували ІЧ-чутливу ПЗЗ камеру та джерело ІЧ (850 нм). Аналіз проводили за допомогою комп'ютерних програм. Для груп зразків різної агресивності раку вираховували середнє співвідношення між показниками, отриманими при дослідженні ділянок з раковими клітинами та ділянок з нормальними клітинами. **Результати**. Співвідношення між показниками, отриманими при дослідженні ділянок із злоякісними клітинами та ділянок з нормальними клітинами в групах зразків раку різної агресивності складало: 6,8—7,2 для низької агресивності, 5,2—6,1 для проміжного ступеня агресивності й 4,4—5,0 для високої агресивності, причому ці діапазони не перекривались. В контрольних зразках тканини це співвідношення перевищувало 7,5. **Висновок**. Візуалізація в ІЧ надійно диференціює зразки пухлинної тканини з різним ступенем агресивності з чутливістю 88% та специфічністю 91%. Цей метод може сприяти ранній діагностиці та вибору персоналізованих стратегій лікування.

Ключові слова: рак передміхурової залози, інфрачервона візуалізація, діагностика.